The Astrophysical Journal, 783:99 (7pp), 2014 March 10 doi:10.1088/0004-637X/783/2/99

ON THE X-RAY VARIABILITY OF MAGNETAR 1RXS J170849.0−400910

P. Scholz[1], R. F. Archibald[1], V. M. Kaspi[1], C.-Y. Ng[1,2], A. P. Beardmore[3], N. Gehrels[4], and J. A. Kennea[5]
[1] Department of Physics, Rutherford Physics Building, McGill University, 3600 University Street, Montreal, Quebec, H3A 2T8, Canada; pscholz@phsyics.mcgill.ca
[2] Department of Physics, The University of Hong Kong, Pokfulam Road, Hong Kong
[3] Department of Physics and Astronomy, University of Leicester, University Road, Leicester LE1 7RH, UK
[4] Astrophysics Science Division, NASA Goddard Space Flight Center, Greenbelt, MD 20771, USA
[5] Department of Astronomy and Astrophysics, 525 Davey Lab, Pennsylvania State University, University Park, PA 16802, USA
Received 2013 October 28; accepted 2014 January 19; published 2014 February 20

ABSTRACT

We present a long-term X-ray flux and spectral analysis for 1RXS J170849.0−400910 using the *Swift*/X-Ray Telescope spanning over eight years from 2005 to 2013. We also analyze two observations from *Chandra* and *XMM* in the period from 2003 to 2004. In this ten-year period, 1RXS J170849.0−400910 displayed several rotational glitches. Previous studies have claimed variations in the X-ray emission associated with some of the glitches. From our analysis we find no evidence for significant X-ray flux variations and evidence for only low-level spectral variations. We also present an updated timing solution for 1RXS J170849.0−400910, from *Rossi X-ray Timing Explorer* and *Swift* observations, which includes a previously unreported glitch at MJD 56019. We discuss the frequency and implications of radiatively quiet glitches in magnetars.

Key words: pulsars: individual (1RXS J170849.0−400910) – stars: neutron – X-rays: general

1. INTRODUCTION

Magnetars are a type of pulsar that exhibit exotic and often violent properties. Their defining characteristic is that they are powered not by their rotation, as are most Crab-like pulsars, but by the decay of their high magnetic fields. Because of the energy provided by the magnetic field decay, their X-ray luminosities are generally higher than their rotational spin-down energies. They often display outburst activity during which they can increase their brightness by an order of magnitude or more and emit short (∼10 ms to ∼1 s in duration) energetic bursts. Previously, magnetars had been classified into two observational categories: anomalous X-ray pulsars (AXPs) and soft-gamma repeaters (SGRs). However, these two "classes" appear to be merely different ends of the magnetar behavioral spectrum. For a review see Woods & Thompson (2006).

Glitches in magnetars have been observed both with and without associated radiative changes. Out of the 26 magnetars and magnetar candidates[6] (Olausen & Kaspi 2014) only five are monitored sufficiently frequently to detect unambiguously the occurrence of glitches (Dib & Kaspi 2014). Of those five, one, 1E 1841−045, has never displayed any radiative activity associated with its glitches (Zhu & Kaspi 2010) whereas 1E 1048.1−5937, 1E 2259+586, and 4U 0142+61 have had radiative events during some or all of their glitches (Dib et al. 2009; Kaspi et al. 2003; Gavriil et al. 2011; Dib & Kaspi 2014). It is important to determine whether or not there is a generic connection between magnetar glitches and radiative events because it can help us determine the physical origin of these phenomena. It seems reasonable that magnetospheric mechanisms, because of their external nature, are likely to be accompanied by radiative changes whereas internal mechanisms could produce radiatively quiet glitches.

1RXS J170849.0−400910 (hereafter referred to as RXS J1708 for brevity) was first identified as an X-ray source in the *ROSAT* all-sky survey (Voges et al. 1999). It was first discovered as a pulsar by Sugizaki et al. (1997), using *ASCA* data, who suggested that it was an AXP based on its X-ray spectrum and 11 s spin period. Israel et al. (1999) measured a period derivative typical of AXPs for RXS J1708, confirming that the source is an AXP, and thus a magnetar.

RXS J1708 was the first magnetar observed to glitch (Kaspi et al. 2000). It has since been found to glitch several more times (Israel et al. 2007; Dib et al. 2008; Dib & Kaspi 2014). Note that some of the glitches reported in Israel et al. (2007) are considered to be glitch candidates in Dib et al. (2008) as they could be consistent with timing noise. Rea et al. (2005) first suggested that RXS J1708 exhibited post-glitch X-ray flux variability based on a 2003 *XMM* observation. They reported an *XMM* flux that was significantly lower than preceding *Chandra* and *BeppoSAX* observations. Further evidence for flux variability was claimed based on additional *Swift* and *INTEGRAL* observations (Campana et al. 2007; Götz et al. 2007; Israel et al. 2007). However, puzzlingly, variability at the level claimed in these studies was not seen in the pulsed count rate as measured by frequent observations with *Rossi X-ray Timing Explorer* (*RXTE*; Dib et al. 2008; Dib & Kaspi 2014).

In this paper we analyze all the available *Swift* X-Ray Telescope (XRT) data from the period of the claimed variability to present day. We also use one *XMM* and one *Chandra* observation that were performed prior to the start of the *Swift* observations. We then use the measured spectral and flux values to constrain the level of source variability. We also present an up-to-date timing solution which continues the *RXTE* timing of Dib & Kaspi (2014) using *Swift*. We then discuss the occurrence of radiatively quiet glitches in magnetars.

2. OBSERVATIONS

2.1. Swift Observations

RXS J1708 was observed by the *Swift* XRT frequently between 2005 and 2010. Beginning in 2011 July, RXS J1708 was observed as a continuation of the *RXTE* timing campaign

[6] See the magnetar catalog at http://www.physics.mcgill.ca/~pulsar/magnetar/main.html.

summarized by Dib & Kaspi (2014). Here we use all available archival *Swift* data in that time period in both Windowed Timing (WT) and Photon Counting (PC) modes. There were 80 observations for a total exposure time of 268 ks. Table 1 shows a summary of the *Swift* observations used in this work.

We downloaded the unfiltered Level 1 data from the *HEASARC* data archive and ran the standard *Swift* data reduction script `xrtpipeline` using the source position of $17^h08^m46^s.87$, $-40°08'52''.44$ (Israel et al. 2003) and the best available spacecraft attitude file. Events were then reduced to the solar-system barycenter using the same position. For WT mode, a 30 pixel long strip centered on the source was used to extract the source events and a 50 pixel long strip positioned away from the source was used to extract the background events. For PC mode observations, an annular region with inner radius 3 pixels and outer radius 20 pixels was used. The inner region was excluded to avoid pileup of the source. An annulus with inner radius 40 pixels and outer radius 60 pixels was used as the background region.

For WT mode data, exposure maps, spectra, and ancillary response files were created for each individual orbit. The spectra and ancillary response files were then summed to create a spectrum for each observation. For the PC mode data, exposure maps, spectra and ancillary response files were created on a per observation basis. We used response files for spectral fitting from the 20120209 CALDB.

The use of exposure maps when creating the ancillary response files is especially important for *Swift* data, as there are columns of bad pixels which can disrupt the point-spread function (PSF) of the source for parts of certain observations. Orbits were not used in the observation if the bad columns were found to be within 3 pixels of the source position.

For WT mode data we selected only Grade 0 events for spectral fitting as higher Grade events are more likely to be caused by a background event (Burrows et al. 2005). In PC mode we used the standard Grade 0-12 selection.

2.2. Chandra and XMM Observations

In this study, we also reprocessed archival data taken with the *Chandra X-ray Observatory* and *XMM-Newton*. To avoid pileup, we used the *Chandra* continuous-clocking (CC) mode observation (ObsID 4605) and the *XMM* PN small-window mode data (ObsID 0148690101). The former was taken on 2004 July 3 with the ACIS-S detector in CC mode, which has a time resolution of 3 ms. The total exposure was 29 ks. The *XMM* observations were made on 2003 August 28. The PN and MOS detectors were run in small and large window modes, with 0.5 s and 6 ms time resolution, respectively. As the source is bright, the low time resolution of the MOS data results in significant pileup. Therefore, we focused only on the PN data. After filtering for periods of high background, we were left with 35 ks of exposure. This is equivalent to 24 ks of live time since the small-window mode has an efficiency of 70%.

We processed the *Chandra* and *XMM* data using CIAO 4.4 and SAS 11, respectively. The source spectrum was extracted using a 6″wide region from the *Chandra* observation and a 40″ radius aperture from the *XMM* PN data. For the *Chandra* observation, the background spectrum was extracted from the entire one-dimensional CC-mode strip excluding the inner 1′ closest to the source. For the *XMM* observation, the background spectrum was extracted from two 40″radius circular regions placed away from the source.

3. ANALYSIS AND RESULTS

3.1. Flux and Spectra

We first fit the spectra for each individual observation with a photoelectrically absorbed power-law model. The spectra were fit with a single N_H using the XSPEC `tbabs` model with abundances from Wilms et al. (2000), and photoelectric cross-sections from Verner et al. (1996). We used XSPEC[7] with Cash statistics (Cash 1979) to fit the spectra because of the low number of counts in the *Swift* observations. The gray points in Figure 1 show the results of the spectral fits to the individual observations. The typical uncertainties in the spectral parameters vary widely due to the large range in exposure times. In order to place the best constraints on the variability, we consider PC and WT modes separately. This is because the two modes are calibrated to within only 10% of each other (A. Beardmore 2013, private communication). The mean and standard deviation of the 1–10 keV absorbed flux for the PC mode data are 4.0×10^{-11} erg cm^{-2} s^{-1} and 1.9×10^{-12} erg cm^{-2} s^{-1}, respectively. The PC mode photon index has a mean and standard deviation of 3.1 and 0.08. For WT mode the mean and standard deviation are 4.0×10^{-11} erg cm^{-2} s^{-1} and 2.1×10^{-12} erg cm^{-2} s^{-1} for flux and 3.2 and 0.07 for the photon index.

In order to better constrain the variability, we then separated the *Swift* spectra into sets of observations nearby in time (see Table 1). Within each set, the 1–10 keV flux and photon-index were consistent with being constant (i.e., the χ^2 values of fits to a mean value in each set were consistent with being drawn from a χ^2 distribution). We fit the sets of *Swift* observations as well as the *XMM* and *Chandra* spectra with a photoelectrically absorbed power law. Each *Swift* set was fitted with the same model with all spectral parameters the same from observation to observation within the set. All parameters were allowed to vary from set to set except for N_H which was tied to the same parameter for all sets and was measured to be $(2.434 \pm 0.008) \times 10^{22}$ cm^{-2}. We did not fit the conventional but more complicated blackbody plus power-law model because the addition of the extra blackbody component did not improve the goodness-of-fit significantly for any of the *Swift* sets. Although additional components are significant for the *XMM* and *Chandra* spectra, we opted to use a single component model because only *Swift* data are used here to constrain the variability (see Section 4.1) and using a single-component model simplifies the comparison of spectral properties. The joint power-law fit to the sets of observations provided a Cash statistic of 32806 and a Pearson χ^2 of 37,191 for 33,571 degrees of freedom. This corresponds to a reduced χ^2 of 1.1.

Figure 1 shows the 1–10 keV absorbed flux and power-law index as a function of time resulting from the spectral fit to the sets. The mean and standard deviation of the flux for the PC mode sets are 4.0×10^{-11} erg cm^{-2} s^{-1} and 8.4×10^{-13} erg cm^{-2} s^{-1}, respectively. The PC mode photon index has a mean and standard deviation of 3.1 and 0.07. Thus for PC mode, the maximum variability allowed by 3σ confidence intervals (three times the standard deviation divided by the average value) is 6.3% for the flux and 7.5% for the photon index. In WT mode, the mean flux is measured to be 4.1×10^{-11} erg cm^{-2} s^{-1} with a standard deviation of 5.9×10^{-13} erg cm^{-2} s^{-1} for a maximum variability of 4.3%. For the photon index, the mean and standard deviation are 3.2

[7] http://heasarc.nasa.gov/xanadu/xspec/

Table 1
Summary of *Swift* Observations of RXS J1708

Sequence	Mode	Observation Date	MJD (TDB)	Exposure Time (ks)	Set	Set Exp. Time (ks)	Set Counts
00050701001	PC	2005 Jan 30	53400.2	2.3			
00050702001	PC	2005 Feb 2	53403.0	4.6			
00050702002	PC	2005 Feb 23	53424.0	2.0	2005	23.1	10947
00050701002	PC	2005 Feb 24	53425.1	11.9			
00050700006	PC	2005 Mar 23	53452.2	2.3			
00035318001	PC	2006 Sep 20	53998.4	2.7	2006	11.8	5081
00035318004	PC	2006 Oct 9	54017.3	9.2			
00035318005	PC	2007 Feb 25	54156.3	1.3			
00035318006	PC	2007 Feb 28	54159.0	1.8			
00035318007	PC	2007 Mar 5	54164.9	2.3			
00035318008	PC	2007 Mar 13	54172.7	1.2	2007	12.4	5537
00035318010	PC	2007 Mar 18	54177.8	2.0			
00035318012	PC	2007 Mar 23	54182.6	2.0			
00035318011	PC	2007 Mar 26	54185.4	1.7			
00035318013	PC	2008 Feb 23	54519.2	15.9	2008-PC	20.9	10169
00090025001	PC	2008 May 13	54599.0	5.0			
00090057001	WT	2008 Apr 2	54558.0	3.0			
00090057002	WT	2008 Apr 3	54559.6	2.1			
00090057003	WT	2008 Apr 4	54560.5	3.2			
00090057004	WT	2008 Apr 8	54564.1	1.2	2008-1	27.1	26586
00090057005	WT	2008 Apr 11	54567.0	3.8			
00090057006	WT	2008 Jun 5	54622.2	6.4			
00090057007	WT	2008 Jun 6	54623.4	7.5			
00090057008	WT	2008 Aug 13	54691.3	7.4			
00090057009	WT	2008 Aug 14	54692.1	1.4	2008-2	16.4	15260
00090057010	WT	2008 Oct 3	54742.0	7.0			
00090057011	WT	2008 Oct 10	54749.7	0.6			
00090057012	WT	2009 Feb 6	54868.3	2.2			
00090057013	WT	2009 Feb 8	54870.1	3.8			
00090057014	WT	2009 Feb 15	54877.1	12.7	2009-1	42.9	42616
00090057015	WT	2009 Mar 20	54910.0	16.5			
00090213001	WT	2009 Apr 26	54947.1	7.7			
00090213002	WT	2009 Jun 28	55010.9	8.7			
00090213004	WT	2009 Sep 2	55076.2	8.7	2009-2	22.3	21748
00090213005	WT	2009 Oct 11	55115.0	4.9			
00090213006	WT	2010 Feb 3	55230.0	8.6			
00090213007	WT	2010 Feb 4	55231.7	5.4	2010	23.8	23038
00090213008	WT	2010 Mar 25	55280.0	9.8			
00035318014	WT	2011 Jul 28	55770.3	0.9			
00035318015	WT	2011 Aug 4	55777.4	1.0			
00035318016	WT	2011 Aug 11	55784.0	2.3			
00035318017	WT	2011 Aug 18	55791.2	1.9			
00035318018	WT	2011 Aug 25	55798.3	2.0			
00035318019	WT	2011 Sep 1	55805.4	2.1			
00035318020	WT	2011 Sep 8	55812.5	2.2	2011	27.8	27744
00035318021	WT	2011 Sep 15	55819.2	2.2			
00035318022	WT	2011 Sep 22	55826.1	2.3			
00035318023	WT	2011 Sep 29	55833.9	2.4			
00035318024	WT	2011 Oct 6	55840.8	2.3			
00035318025	WT	2011 Oct 13	55847.0	1.6			
00035318026	WT	2011 Oct 20	55854.3	0.9			
00035318027	WT	2011 Oct 22	55856.3	1.8			
00035318028	WT	2011 Oct 27	55861.1	2.0			
00035318029	WT	2012 Jan 25	55951.5	2.0			
00035318030	WT	2012 Feb 1	55958.3	2.1			
00035318031	WT	2012 Feb 8	55965.8	2.2			
00035318032	WT	2012 Feb 15	55972.2	0.3			
00035318033	WT	2012 Feb 22	55979.8	0.4			
00035318034	WT	2012 Feb 29	55986.4	2.2			

Table 1
(Continued)

Sequence	Mode	Observation Date	MJD (TDB)	Exposure Time (ks)	Set	Set Exp. Time (ks)	Set Counts
00035318035	WT	2012 Mar 7	55993.3	2.2	2012-1	21.0	21056
00035318036	WT	2012 Mar 16	56002.6	2.2			
00035318037	WT	2012 Mar 21	56007.5	1.0			
00035318038	WT	2012 Mar 28	56014.9	1.6			
00035318039	WT	2012 Apr 13	56030.2	1.6			
00035318040	WT	2012 Apr 26	56043.1	1.5			
00035318041	WT	2012 May 10	56057.3	1.3			
00035318042	WT	2012 May 25	56072.0	0.5			
00035318043	WT	2012 Jun 7	56085.6	2.0	2012-2	10.8	11423
00035318044	WT	2012 Jun 22	56100.2	1.5			
00035318045	WT	2012 Jul 5	56113.4	0.6			
00035318047	WT	2012 Jul 15	56123.5	1.1			
00035318048	WT	2012 Aug 16	56155.0	1.7			
00035318049	WT	2012 Sep 6	56176.1	2.0			
00035318050	WT	2012 Sep 27	56197.1	1.7			
00035318052	WT	2012 Oct 23	56223.4	0.3			
00035318053	WT	2013 Jan 24	56316.3	1.0	2013	7.1	7380
00035318054	WT	2013 Feb 13	56336.8	1.9			
00035318055	WT	2013 Mar 6	56357.1	2.0			
00035318056	WT	2013 Mar 27	56378.6	0.7			
00035318057	WT	2013 Mar 31	56382.2	1.5			

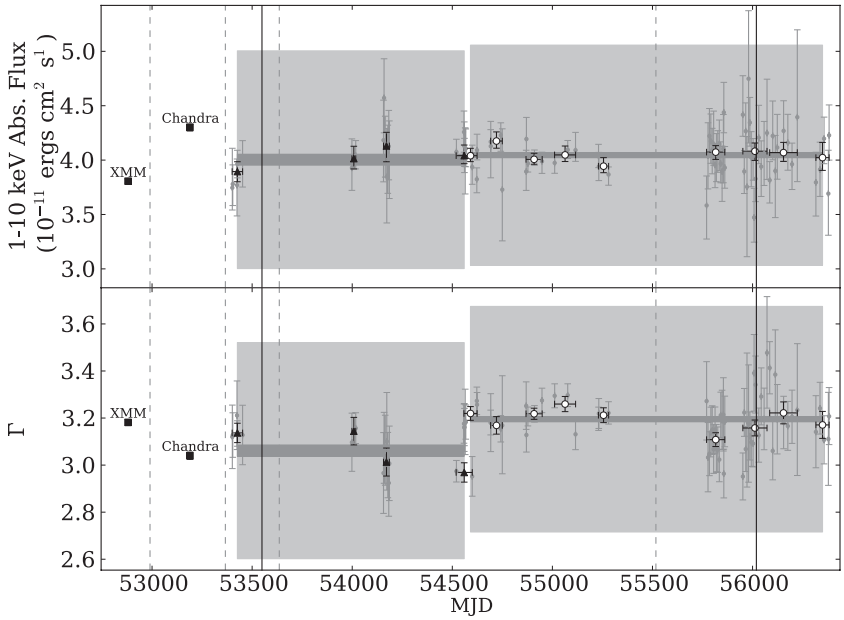

Figure 1. Top panel: absorbed 1–10 keV flux of RXS J1708 over a ∼10 yr period. Note that the zero on the *y*-axis is suppressed. Bottom panel: photon indices from fitting a power-law model to the 1–10 keV spectrum. Gray points are from spectral fits to individual observations. Black triangles are sets of *Swift* PC mode observations, and white circles are sets of *Swift* WT mode observations (see Table 1 for definitions of sets). *XMM* and *Chandra* observations are labeled. The dark gray bands represent the 90% error in the mean and the light gray bands represent the level of previously claimed variability (∼50% in 1–10 keV flux and ∼30% in spectral index; Götz et al. 2007). The solid vertical lines represent the epochs of glitches and the dashed lines indicate the epochs of glitch candidates. All error bars are 90% confidence intervals.

and 0.04 for a maximum variability of 4.0%. Compared to the standard deviations measured for the individual observations above, the constraints here from fitting the sets of observations improved as little as a factor of 1.2 (PC mode photon-index) and as much as a factor of 3.5 (WT mode flux). A greater improvement is achieved with WT mode than PC mode, which makes sense given that the individual WT mode observations have a large number of short ($\lesssim$2 ks) observations.

The probability of the data being constant can be estimated from the χ^2 of each data set. For the PC mode observation sets, the reduced χ^2_ν/ν for the flux is 2.4/3 which corresponds to a 6.7% probability of being constant and for the power-law index the χ^2_ν/ν is 11/3 (5.1×10^{-5}% probability). The sets of WT mode observations have a χ^2_ν/ν of 2.3/8 (2.1% probability) for flux and a χ^2_ν/ν of 6.1/8 (6.3×10^{-6}% probability) for power-law index. So, in both modes, the fluxes are consistent

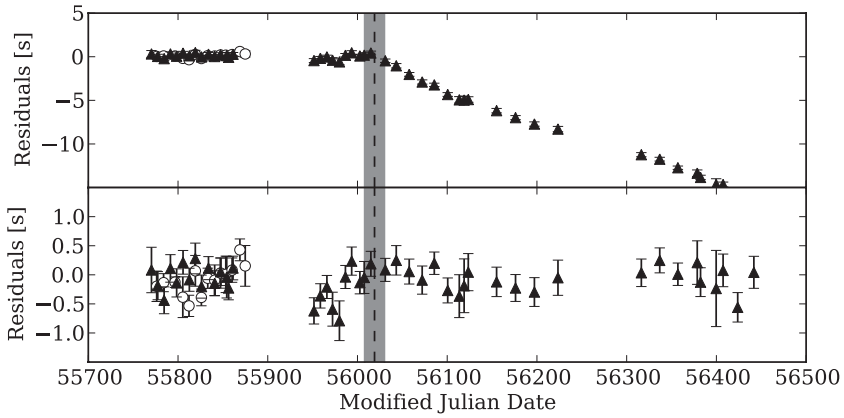

Figure 2. Timing residuals, the difference between the predicted and measured TOAs for the timing model shown in Table 2. The top panel shows residuals before fitting for a glitch, and the bottom panel after. In both panels, open circles indicate data from *RXTE*, and black triangles indicate *Swift*. The vertical dashed line represents the glitch epoch and the gray band represents the uncertainty in that epoch.

with being constant (i.e., within 3σ), although the power-law indices are only consistent within a 5σ tolerance. This could be due to unknown systematic sources of error or possibly low-level spectral variations, possibly due to the neglected blackbody component. Regardless, these variations are much lower than the ∼30% previously claimed (Rea et al. 2005; Campana et al. 2007; Götz et al. 2007).

3.2. Timing

A phase-coherent timing solution for RXS J1708 has been maintained using *RXTE* since 1998; see Dib & Kaspi (2014). In order to continue to maintain a timing solution for RXS J1708, we began a monitoring campaign using the *Swift*/XRT on 2011 July 28, overlapping with the *RXTE* campaign, until *RXTE*'s demise in 2011 December. Monitoring observations were typically 2 ks long. Barycentered events were used to derive a pulse time of arrival (TOA) for each observation. For a given observation, a TOA was obtained using a maximum likelihood (ML) method, as described by Livingstone et al. (2009) and Scholz et al. (2012). The ML method compares a continuous model of the pulse profile, derived from taking aligned profiles of all the pre-glitch *Swift*/XRT observations, and creating a template composed of the first five Fourier components.

These TOAs were fitted to a pulse arrival time model in which the phase, ϕ, at time t is given by:

$$\phi(t) = \phi_0 + \nu_0(t - t_0) + \frac{1}{2}\dot{\nu}_0(t - t_0)^2, \quad (1)$$

where ϕ_0, ν_0, and $\dot{\nu}_0$ are the phase, frequency, and frequency derivative of the pulsar respectively at the reference epoch t_0. This was accomplished using the TEMPO2 (Hobbs et al. 2006) pulsar timing software package.

In Figure 2 we show the timing residuals for RXS J1708 starting on 2011 July 28 and show the overlap between the *RXTE* and *Swift* monitoring epochs. The data are well fit by a single spin frequency and frequency derivative (Table 2). However, we identified one notable timing event which we report as a new glitch. The event occurred within 11 days (1σ uncertainty) of MJD 56019 with a decaying $\Delta\nu/\nu = (8.3 \pm 0.6) \times 10^{-7}$. The glitch displayed an exponential recovery with a timescale of 111 ± 15 days, 2.6 ± 0.3 times longer than the 43 ± 2 day decay time of the other reported decaying glitch in the source (Dib et al. 2008). This glitch was accompanied by a $\Delta\dot{\nu}$ of $(1.4 \pm 0.3) \times 10^{-15}$ Hz s^{-1}.

Table 2
Timing Parameters for RXS J1708

Parameter	Value
Observation dates	2011 July 28–2013 May 29
Dates (MJD)	55770.396 – 56441.770
Epoch (MJD)	56000.000
Number of TOAs	61
ν (s^{-1})	0.090851264(3)
$\dot{\nu}$ (s^{-2})	$-1.638(3) \times 10^{-13}$
Glitch	
Glitch epoch (MJD)	56019(11)
$\Delta\nu_d$ (s^{-1})	$7.5(5) \times 10^{-8}$
τ_d (days)	111(15)
$\Delta\dot{\nu}$ (s^{-2})	$1.4(3) \times 10^{-15}$
rms residuals (ms)	229.07
χ^2/ν	64.94/55

Note. Numbers in parentheses are TEMPO2 reported 1σ uncertainties.

4. DISCUSSION

In this paper, we have reported on the flux and spectral properties of RXS J1708 over a ∼10 yr period from 2003 to 2013. We show that there is no significant flux variability and that only low-level spectral variations are seen. We have also presented an up-to-date timing solution and we report on a glitch that occurred on MJD ∼ 56019. Below we compare our findings with previous results and discuss the significance of the lack of variability in RXS J1708.

4.1. Flux Variability of RXS J1708

In this work, we do not use measured flux and spectral properties between different X-ray telescopes to constrain the variability of RXS J1708. This is because cross-calibration between instruments onboard the *Swift*, *Chandra*, and *XMM* telescopes is such that the flux and spectral index can differ by up to 20% and 9%, respectively (e.g., Tsujimoto et al. 2011). As seen in Figure 1, the *XMM* and *Chandra* observations are consistent with one another within those tolerances. Additionally, each *Swift* XRT mode (PC and WT) is considered separately, as the

two modes are cross-calibrated only to within 10% in flux (A. Beardmore 2013, private communication).

Previous studies have claimed that RXS J1708 displayed variability following glitches that occurred between 2002 and 2005. Using a multi-component blackbody plus power-law model, Götz et al. (2007) measure a low 1–10 keV absorbed flux of $\sim 3 \times 10^{-11}$ erg cm^{-2} s^{-1} for the 2003 *XMM* observation and 2006 set of *Swift* observations. They measured a higher flux for the 2004 *Chandra* observation and the 2005 set of *Swift* observations. Their highest flux measured is $\sim 4.5 \times 10^{-11}$ erg cm^{-2} s^{-1} for the 2005 *Swift* set. This gives a total claimed variability of $\sim$50%.

Because we used a single-component model in Section 3.1, the values in Figure 1 are not directly comparable to those in Götz et al. (2007). For the *Swift* data, additional spectral components do not significantly improve the fit. However, additional components for *Chandra* and *XMM* observations do provide a much better fit and so here we apply a blackbody plus power-law model for direct comparison with Götz et al. (2007). With a multi-component model we measure 1–10 keV absorbed fluxes of $(3.83 \pm 0.04) \times 10^{-11}$ erg cm^{-2} s^{-1} for the *XMM* spectrum and $(4.29 \pm 0.08) \times 10^{-11}$ erg cm^{-2} s^{-1} for the *Chandra* observation. This 11% discrepancy in flux between the two observations is within the 20% cross-calibration error. As in Götz et al. (2007), we find that the temperature of the blackbody component of the model is consistent between the two observations and is 0.46 ± 0.01 keV. For the photon index we measure 2.63 ± 0.03 and 2.50 ± 0.07 for the *XMM* and *Chandra* observations, respectively. This compares to $\Gamma \sim 2.8$ for both observations in Götz et al. (2007). Reassuringly, the *Chandra* flux that we measure is higher than the *XMM* flux and the *Chandra* spectral index is harder as found in cross-calibration studies (e.g., Tsujimoto et al. 2011).

In order to attempt to reproduce previous *Swift* results, for which only PC mode data were used (Götz et al. 2007), we processed the PC mode data from 2005 to 2007 without using exposure maps and without removing orbits with bad columns within 3 pixels of the center of the PSF. We found the same trend as in previous studies: the flux of the 2005 set of observations was higher than the 2006 and 2007 sets and the flux of the 2007 set was slightly higher than that of the 2006 set. We also observed an apparent correlation between the flux and power-law index. However, the level of variability in the three flux points was only about 30% compared to $\sim$50% claimed in Götz et al. (2007). Still, this is much higher than the $<$10% that we find in our more detailed analysis.

The lack of variability found here using soft X-ray imaging telescopes is consistent with what has been found by non-focusing telescopes in other regimes. Using *INTEGRAL* data, den Hartog et al. (2008) found no significant variability in the hard X-ray flux or spectral index for data spanning from 2003 to 2006. With *RXTE*, Dib et al. (2008) found that the pulsed count rate showed evidence for only low-level variability ($<$15%) and they concluded that the glitches of RXS J1708 appeared to be "quiet," i.e., unassociated with significant changes in the radiative properties of the magnetar.

4.2. Radiative Activity and Glitches in Magnetars

Radiative activity in magnetars is almost always associated with changes in timing behavior (e.g., glitches or increased timing noise; Dib & Kaspi 2014). Of the 26 known magnetars and magnetar candidates, only five have long-term ($<$10 yr) phase-connected timing solutions that can be used to unambiguously detect glitches. These five magnetars are 1E 1841−045, 1E 2259+586, 4U 0142+61, 1E 1048.1−5937, and RXS J1708. Of the three glitches each that have been detected from 1E 2259+586 and 1E 1048.1−5937, five were radiatively loud, with the 2006 glitch of 1E 2259+586 being the exception. The magnetars 1E 1841−045, 4U 0142+61, and RXS J1708 have not displayed any significant flux increases associated with their glitches, although 4U 0142+61 emitted short X-ray bursts near the epoch of its 2006 candidate glitch (see Dib & Kaspi 2014, and references therein).

It is therefore clear that glitches are not always accompanied by radiative changes. Because changes in the magnetosphere would likely manifest as pulse profile or flux variations, it seems more likely that radiatively quiet magnetar glitches have their origin in the interior of the neutron star. If we assume that radiatively quiet and loud glitches have the same origin, a mechanism must exist to allow magnetars to exhibit prompt X-ray flux increases in some cases and no significant flux increases in others.

One possible way to achieve both radiatively loud and quiet glitches in an interior model is to vary the depth at which the glitch-inducing event occurs. Eichler & Cheng (1989) showed that if energy is injected into the crust of a neutron star it can travel outward, and manifest as a prompt outburst, or travel inward and heat the core of the neutron star. The direction of travel depends on the size and depth of the energy deposition. In the inward case, the heat is released slowly over a time scale of thousands of years. The flux decays of magnetars following prompt outbursts are indeed reasonably well modeled by crustal cooling (Lyubarsky et al. 2002; Scholz et al. 2012, 2013; An et al. 2013). If the mechanism that causes glitches in magnetars injects energy at a shallow depth, a radiatively loud glitch would occur.

An additional possible limit to the occurrence of radiative outbursts from magnetars at glitch epochs is the predominance of neutrino emission at high temperatures in neutron star crusts (Eichler & Cheng 1989; van Riper 1991). We expect neutron stars to have a limiting luminosity which occurs when the emission of neutrinos dominates as a cooling mechanism over the emission of photons. We would thus expect the brightest magnetars to be unable to increase their luminosity beyond $\sim 10^{35}$ erg s^{-1} (Thompson & Duncan 1996). The five brightest magnetars, for which long-term timing solutions are available, have luminosities $\sim 10^{35}$ erg s^{-1} (though see below for caveats on luminosity measurements). So, flux increases for these magnetars should either not occur or be small. Indeed, of the five, only 1E 2259+586 and 1E 1048.1−5937 have displayed significant flux increases at glitch epochs (Woods et al. 2004; Gavriil & Kaspi 2004; Tam et al. 2008) and those flux increases were much smaller than those from outbursts observed in fainter transient magnetars (e.g., Israel et al. 2007; Scholz & Kaspi 2011).

However, magnetar luminosities are not well constrained since the source distances are hard to determine. There exist in the literature several disagreements in the distances to magnetars that lead to a discrepancy of up to a factor of $\sim$30 in luminosity (e.g., see An et al. 2012 versus Durant & van Kerkwijk 2006 for 1E 1048.1−5937). Even when the distance is agreed upon there are discrepancies. For example, for RXS J1708, the only distance estimation is from Durant & van Kerkwijk (2006) but the 2–10 keV luminosity has been reported to be as low as 4.2×10^{34} erg s^{-1} (Olausen & Kaspi 2014) and as high as 1.4×10^{35} erg s^{-1} (Rea & Esposito 2011). From the model given by our best-fit mean flux and spectral indices, we get a 2–10 keV unabsorbed flux of 3.9×10^{-11} erg cm^{-2} s^{-1}, which corresponds

to a 2–10 keV luminosity of 6.8×10^{34} erg s^{-1}, closer to that listed in the magnetar catalog (Olausen & Kaspi 2014). Discrepancies such as this could be caused by the difference in spectral models used or differences in the instruments used to measure the flux (as mentioned above, X-ray detector cross-calibration can be discrepant up to 20%). We therefore cannot say conclusively whether magnetar luminosity is inversely correlated with the size of radiative activity as discussed here and as previously proposed in Pons & Rea (2012).

If we do assume that fainter magnetars are able to have larger flux increases coincident with glitches, this suggests a rough luminosity order for the five brightest magnetars. RXS J1708, 1E 1841−045, and 4U 0142+61 have experienced only radiatively quiet glitches whereas 1E 1048.1−5937 and 1E 2259+586 have shown significant flux increases during some (or all for 1E 1048.1−5937) of their glitches. That suggests that RXS J1708, 1E 1841−045, and 4U 0142+61 are more luminous than the other two.

Pulsars with higher *B*-fields are expected to be more luminous and have higher surface temperatures than pulsars with lower magnetic fields because of energy deposition from the decay of their magnetic fields. Indeed, it has been shown that high-*B* radio pulsars are systematically hotter than similarly aged pulsars with lower magnetic fields (Zhu et al. 2011; Olausen et al. 2013). We may also expect that magnetar-like activity in such sources could arise due to energy from the magnetic field being deposited at shallow depths. Case in point, the high-*B* rotation-powered pulsar PSR J1846−0258 displayed a magnetar-like outburst in 2006 (Gavriil et al. 2008). In recent years, two magnetars, SGR 0418+5729 and Swift J1822.3−1606, were discovered with magnetic fields lower than several high-*B* rotation-powered pulsars and have had clear X-ray outbursts (though it is unknown whether or not they accompanied glitches; Rea et al. 2010; Livingstone et al. 2011). It is thus becoming increasingly clear that high-*B* rotation powered pulsars and magnetars are related and form a spectrum of objects rather than two distinct groups. Therefore, the mechanism that causes X-ray outbursts at glitch epochs could be active in all high-*B* field pulsars.

5. CONCLUSIONS

We have presented an analysis of all of the *Swift* WT and PC mode data of RXS J1708 in the period 2005–2013. We show that the maximum variability for both the 1–10 keV X-ray flux and spectral index is constrained to <10%. This is much less than claimed by previous studies and is consistent with the flux being constant. We also report on a newly discovered glitch at MJD $\sim$ 56019 which has a fractional amplitude of $\Delta\nu/\nu = (8.3 \pm 0.6) \times 10^{-7}$, typical of magnetar glitches.

The occurrence of both radiatively quiet and loud glitches in magnetars, sometimes from the same source, shows that the mechanism that causes these glitches must be able to produce prompt flux increases in some cases and no significant increases in others. Here we have discussed the possibility that the glitches originate internally to the neutron star, with the deciding factor the depth of the energy deposition associated with the glitch. We note that these conclusions have been drawn from a sample of only five magnetars and therefore increasing the number of magnetars for which we can unambiguously detect glitches would be beneficial in answering the questions posed here.

We are grateful to the *Swift* team for their flexibility in the scheduling of the timing monitoring campaign of RXS J1708. We thank Marten van Kerkwijk, Andrew Cumming, Dave Tsang, and Kostas Gourgouliatos for helpful discussions. V.M.K. holds the Lorne Trottier Chair in Astrophysics and Cosmology and a Canadian Research Chair in Observational Astrophysics. R.F.A. receives support from a Walter C. Sumner Memorial Fellowship. This work is supported by NSERC via a Discovery Grant and an Accelerator Supplement, by FQRNT via the Centre de Recherche en Astrophysique du Québec, and by the Canadian Institute for Advanced Research.

REFERENCES

An, H., Kaspi, V. M., Archibald, R., & Cumming, A. 2013, ApJ, 763, 82
An, H., Kaspi, V. M., Tomsick, J. A., et al. 2012, ApJ, 757, 68
Burrows, D. N., Hill, J. E., Nousek, J. A., et al. 2005, SSRv, 120, 165
Campana, S., Rea, N., Israel, G. L., Turolla, R., & Zane, S. 2007, A&A, 463, 1047
Cash, W. 1979, ApJ, 228, 939
den Hartog, P. R., Kuiper, L., & Hermsen, W. 2008, A&A, 489, 263
Dib, R., & Kaspi, V. M. 2014, ApJ, submitted (arXiv:1401.3085)
Dib, R., Kaspi, V. M., & Gavriil, F. P. 2008, ApJ, 673, 1044
Dib, R., Kaspi, V. M., & Gavriil, F. P. 2009, ApJ, 702, 614
Durant, M., & van Kerkwijk, M. H. 2006, ApJ, 650, 1070
Eichler, D., & Cheng, A. F. 1989, ApJ, 336, 360
Gavriil, F. P., Dib, R., & Kaspi, V. M. 2011, ApJ, 736, 138
Gavriil, F. P., Gonzalez, M. E., Gotthelf, E. V., et al. 2008, Sci, 319, 1802
Gavriil, F. P., & Kaspi, V. M. 2004, ApJL, 609, L67
Götz, D., Rea, N., Israel, G. L., et al. 2007, A&A, 475, 317
Hobbs, G. M., Edwards, R. T., & Manchester, R. N. 2006, MNRAS, 369, 655
Israel, G. L., Campana, S., Dall'Osso, S., et al. 2007, ApJ, 664, 448
Israel, G. L., Covino, S., Perna, R., et al. 2003, ApJL, 589, L93
Israel, G. L., Covino, S., Stella, L., et al. 1999, ApJL, 518, L107
Israel, G. L., Götz, D., Zane, S., et al. 2007, A&A, 476, L9
Kaspi, V. M., Gavriil, F. P., Woods, P. M., et al. 2003, ApJL, 588, L93
Kaspi, V. M., Lackey, J. R., & Chakrabarty, D. 2000, ApJL, 537, L31
Livingstone, M. A., Ransom, S. M., Camilo, F., et al. 2009, ApJ, 706, 1163
Livingstone, M. A., Scholz, P., Kaspi, V. M., Ng, C.-Y., & Gavriil, F. P. 2011, ApJL, 743, L38
Lyubarsky, Y., Eichler, D., & Thompson, C. 2002, ApJL, 580, L69
Olausen, S. A., & Kaspi, V. M. 2014, ApJS, submitted (arXiv:1309.4167)
Olausen, S. A., Zhu, W. W., Vogel, J. K., et al. 2013, ApJ, 764, 1
Pons, J. A., & Rea, N. 2012, ApJL, 750, L6
Rea, N., & Esposito, P. 2011, in Astrophysics and Space Science Proceedings, High-Energy Emission from Pulsars and their Systems, ed. D. F. Torres & N. Rea (Berlin: Springer), 247
Rea, N., Esposito, P., Turolla, R., et al. 2010, Sci, 330, 944
Rea, N., Oosterbroek, T., Zane, S., et al. 2005, MNRAS, 361, 710
Scholz, P., & Kaspi, V. M. 2011, ApJ, 739, 94
Scholz, P., Kaspi, V. M., & Cumming, A. 2014, ApJ, submitted (arXiv:1401.6965)
Scholz, P., Ng, C.-Y., Livingstone, M. A., et al. 2012, ApJ, 761, 66
Sugizaki, M., Nagase, F., Torii, K. I., et al. 1997, PASJ, 49, L25
Tam, C. R., Gavriil, F. P., Dib, R., et al. 2008, ApJ, 677, 503
Thompson, C., & Duncan, R. C. 1996, ApJ, 473, 322
Tsujimoto, M., Guainazzi, M., Plucinsky, P. P., et al. 2011, A&A, 525, A25
van Riper, K. A. 1991, ApJ, 372, 251
Verner, D. A., Ferland, G. J., Korista, K. T., & Yakovlev, D. G. 1996, ApJ, 465, 487
Voges, W., Aschenbach, B., Boller, T., et al. 1999, A&A, 349, 389
Wilms, J., Allen, A., & McCray, R. 2000, ApJ, 542, 914
Woods, P. M., Kaspi, V. M., Thompson, C., et al. 2004, ApJ, 605, 378
Woods, P. M., & Thompson, C. 2006, in Compact Stellar X-ray Sources, ed. W. H. G. Lewin & M. van der Klis (Cambridge: Cambridge Univ. Press), 547
Zhu, W., & Kaspi, V. M. 2010, ApJ, 719, 351
Zhu, W. W., Kaspi, V. M., McLaughlin, M. A., et al. 2011, ApJ, 734, 44